

Peculiarities of the hydrogenated In(AsN) alloy

S. Birindelli¹, M. Kesaria², D. Giubertoni³, G. Pettinari⁴, A. V. Velichko⁵, Q. D. Zhuang², A. Krier², A. Patanè⁵, A. Polimeni¹ and M. Capizzi^{1,(a)}

¹Dipartimento di Fisica and CNISM, Sapienza Università di Roma, Piazzale A. Moro 2, 00185
Roma, Italy

²Physics Department, Lancaster University, Lancaster LA1 4YB, UK

³Center for Materials and Microsystems, Fondazione Bruno Kessler, Via Sommarive 18, 38123,
Povo, Trento, Italy

⁴National Research Council, Institute for Photonics and Nanotechnologies,
Via Cineto Romano 42, 00156 Roma, Italy

⁵School of Physics and Astronomy, The University of Nottingham, Nottingham NG7 2RD, UK

(a) mario.capizzi@roma1.infn.it

Abstract. The electronic properties of In(AsN) before and after post-growth sample irradiation with increasing doses of atomic hydrogen have been investigated by photoluminescence. The electron density increases in In(AsN) but not in N-free InAs, until a Fermi stabilization energy is established. A hydrogen $\varepsilon^{+/-}$ transition level just below the conduction band minimum accounts for the dependence of donor formation on N, in agreement with a recent theoretical report highlighting the peculiarity of InAs among III-V compounds. Raman scattering measurements indicate the formation of N-H complexes that are stable under thermal annealing up to ~500 K. Finally, hydrogen does not passivate the electronic activity of N, thus leaving the band gap energy of In(AsN) unchanged, once more in stark contrast to what reported in other dilute nitride alloys.

Keywords: In(AsN), dilute nitrides, hydrogen related complexes, Fermi stabilization energy, electronic properties

1. Introduction

Hydrogen, the smallest and one of the most electronically active atoms, is a common impurity in semiconductors and is virtually present in every step of III-V material growth and device processing. [1] The effects hydrogen has on the transport and optical properties of semiconductor materials have been investigated extensively, with quite unexpected results. [2, 3] Upon hydrogen irradiation dangling bonds are saturated; conductive graphene is turned into an insulator; [4] *p*-type conductivity of diamond is switched to *n*-type; [5] Mn ferromagnetism in Ga(AsMn) is neutralized. [6] Hydrogen has also a “negative U” behavior in a vast class of materials, with a universal pinning level [7, 8] that accounts for an unintentional doping in GaSb, [8] InN, [9, 10], and (InGa)N, [11] as well as for an amphoteric behavior in GaN. [9, 12] Moreover, it has been recently predicted that the transfer level $\epsilon^{+/-}$ of a H atom adsorbed on a semiconductor's surface –namely, the level at which the stable H charge switches from +1 to -1– depends on the specific material investigated, in contrast to what reported in the bulk case. [13]

Even more surprising are the effects that H irradiation has on the structural, electronic, and transport properties of dilute nitrides alloys, such as Ga(AsN), Ga(PN), and (InGa)(AsN). [14] The properties of the host material are severely modified by the substitution of a small percentage of the anions with N, while they are fully recovered upon hydrogenation. [15, 16, 17] This unexpected “passivation” of the electronic activity of N atoms has been theoretically accounted for [18, 19, 20] and experimentally verified [21] by the formation of different N-H_n complexes ($n \geq 2$). These effects have been exploited for hydrogen-assisted band-gap engineering at the nanoscale level, which is a promising alternative to other commonly followed approaches. [22, 23]

Amongst the material operating in the mid-infrared spectral region, there is an increasing interest in InAs, whose band gap energy ($E_g=0.42$ eV at $T=4.2$ K) decreases with increasing the concentration of N [24] or Bi [25] alloying. This makes this material a potential candidate for the realization of optoelectronic devices operating with effective electrical isolation and optical transparency in the mid-infrared spectral region. Therefore, InAs could be exploited for

atmospheric pollution monitoring and industrial process control, as well as for thermal imaging applications. Good quality In(AsN) epilayers with a small concentration of activated nitrogen atoms have been grown on semi-insulating GaAs, [26] thus providing a valuable alternative to the more expensive growth on InP [27] or InAs [28] substrates. However, the large lattice mismatch ($\sim 7.2\%$) [29] between the In(AsN) epilayer and the GaAs substrate, as well as a tendency for N to segregate, lead to the formation of carrier traps and recombination centers —mainly extensive interface defects and dislocations— that strongly reduce the material photoluminescence (PL) efficiency. [24, 30]

In spite of the interest in the optimization of the In(AsN) optical properties, the knowledge of the effects hydrogen has on the electronic properties of this semiconductor is still poor, with scattered experimental results. Room temperature PL efficiency increases by an order-of-magnitude in InAs/GaAs quantum dots when irradiated *in-situ* with atomic hydrogen during the growth, while *post-growth* irradiation with molecular hydrogen has a detrimental effect on PL. [31] On the contrary, post-growth hydrogenation dramatically increases the PL intensity in highly strained, N-free, InAs/GaAs quantum wells. [32] The free-carrier density is also differently affected by hydrogenation: It increases by less than [33] (or about [34]) one order of magnitude in N-free InAs epilayers, while it increases by up to two orders of magnitude, as shown in the In(AsN) alloy by Hall Effect, Shubnikov de Haas oscillations, and Raman scattering, *with no increase in the electron scattering time*. [33, 35]

In the present work, we report on an extensive investigation of the PL properties of In(AsN) as a function of nitrogen content, hydrogenation temperature (T_H), and dose of H irradiation (d_H). First, we show that hydrogen does not neutralize the electronic activity of nitrogen, in stark contrast to the case of other dilute nitride alloys. [14-17, 22] Secondly, a large increase in carrier density is observed upon sample hydrogenation, but not in N-free InAs. Raman scattering measurements support the formation of H-N donor complexes, whose absence in InAs can be accounted for by a hydrogen $\varepsilon^{+/-}$ transition level just below the conduction band minimum.

Isochronal thermal annealing cycles show that the H-N donor complexes are stable up to ~500 K. A well-defined Fermi stabilization energy is achieved upon sample irradiation with high H doses, [36] as indicated by the observation of a Fermi energy independent of N content. Finally, deuterium diffusion profiles obtained with secondary ion mass spectrometry, SIMS, show that increases in carrier density are revealed by PL measurements only when H atoms diffuse into most of the sample, as also supported by PL measurements in samples with different thicknesses. This donor “transparency” in PL can be accounted for by a built-in electric field, most likely because of a pinning of the Fermi energy at the sample surface where a carrier accumulation layer is usually found. [37]

2. Experimental details

A series of thick (~1 μm) $\text{InAs}_{1-x}\text{N}_x$ epilayers, with an *effective* N concentration $x=0, 0.0002, 0.0003, 0.0015, 0.006, 0.011,$ and $0.019,$ as well as a series of thin ($0.33 \mu\text{m}$) samples, with $x=0.002, 0.0025,$ and 0.010 were grown by molecular beam epitaxy on semi-insulating (100) GaAs substrates held at a growth temperature between $380 \text{ }^\circ\text{C}$ and $400 \text{ }^\circ\text{C},$ depending on the N content. The effective N content was estimated from the PL peak energy at $T = 10 \text{ K}$ and low excitation power-density ($P \sim 1 \text{ W}\cdot\text{cm}^{-2}$). According to the Band Anticrossing (BAC) model, [38] indeed, the N concentration is given by $[\text{N}] = (E_g(0) - E_g) \times (E_N - E_g) / (V_N)^2,$ where E_g is the PL peak of the sample under investigation, $E_g(0)$ is the energy gap of the N-free InAs (0.416 eV), E_N is the energy of the isolated N level (1.44 eV [39]), and V_N accounts for the interaction between the N level and the conduction band minimum of the host (2.5 eV [40]). For almost all the samples the $[\text{N}]$ content determined by PL was found to be in good agreement with the nominal value as determined by X ray diffraction. Growth details have been reported elsewhere. [41] The samples were irradiated using a low energy (100 eV) Kaufman source (with ion current densities of a few $\mu\text{A}\cdot\text{cm}^{-2}$ and H doses varying from $d_{\text{H}}=0.5 \times 10^{16}$ to $80 \times 10^{16} \text{ ions}\cdot\text{cm}^{-2}$) to minimize possible damage due to the impinging H ions. During the hydrogenation process, hydrogen diffusion into

the sample was promoted by heating the samples at temperatures (T_H) ranging from 250 °C to 375 °C. Deuterium diffusion profiles were determined by SIMS in samples with $x=0.0015$ (in SIMS measurements, deuterium gives rise to a background signal smaller than that due to hydrogen). Negative secondary ions ($^2\text{H}^-$, $^{75}\text{As}^-$, $^{115}\text{In}^-$, and $^{75}\text{As}^{14}\text{N}^-$) were collected by bombarding the samples with a 1 keV Cs^+ beam at oblique incidence (55°) in a CAMECA Sc-Ultra mass spectrometer. Whenever a higher spatial resolution was required, the energy of the Cs^+ beam was reduced to 0.5 keV. An Ar-ion laser ($\lambda=515$ nm) was used to excite the samples in PL measurements. The emitted light was collected by CaF_2 lenses, spectrally analyzed by a high throughput 0.3-m focal-length monochromator, detected by a liquid-nitrogen cooled InSb photodiode, and measured by a lock-in amplifier. PL spectra at different excitation power (P) were taken for each sample before and after H irradiation. Micro-Raman scattering measurements were taken using a confocal optical microscope equipped with a nano-focusing system, a spectrometer having a 1200 g/mm grating, and a charge-coupled device. Excitation was provided by a He-Ne laser ($\lambda = 633$ nm) focused to a $\sim 1 \mu\text{m}$ diameter by a $100\times$ objective.

3. Experimental results

3.1. Photoluminescence

Photoluminescence spectra taken at 10 K from samples irradiated at $T_H=250$ °C with increasing H doses are shown in Fig. 1 for a N-free sample and for a sample containing a tiny amount of N ($x=0.0002$). In the *N-free* sample, as shown in Fig. 1 (a), the PL signal initially increases upon H irradiation —up to a factor of 9 for $d_H=10\times 10^{16}$ ions- cm^{-2} ($10 H_0$)— and then it decreases. The increased broadening on the low-energy side of the PL band is most likely due to a greater contribution from localized states. No increase in carrier density can be inferred by the PL spectra line-shape at $T_H=250$ °C, at higher T_H 's (not shown here), or for H doses greater than those shown in the figure (for which the PL signal decreases rapidly, most likely because of an increasing weight of defects related to the sample irradiation with H). However, as shown in Fig. 1 (b),

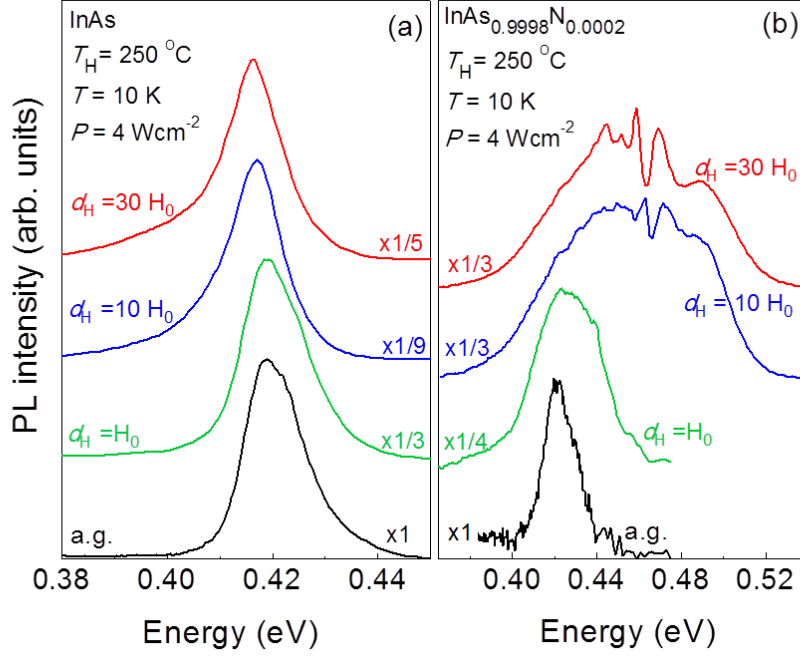


Figure 1. (color online) Peak normalized PL spectra taken at $T=10$ K ($P=4$ Wcm $^{-2}$) for increasing doses of impinging H ions ($H_0=1\times 10^{16}$ ions·cm $^{-2}$) in two 1 μ m-thick samples: (a) InAs, and (b) an InAs $_{0.9998}$ N $_{0.0002}$ sample, both irradiated at $T_H=250$ °C. The dips on the high energy side of the PL spectra are due to atmospheric air absorption. Renormalization factors are indicated for each spectrum. a.g. labels the as-grown samples.

completely different results are obtained in the N -containing sample ($x=0.0002$) upon the same hydrogen treatments. At low H dose ($d_H = 1\times 10^{16}$ ions·cm $^{-2}$), the PL intensity increases (by a factor of 4) and the spectrum broadens, *on both the low and the high energy sides*. For $d_H > 1\times 10^{16}$ ions·cm $^{-2}$, the PL line-shape changes dramatically: The blue-shift of the high energy side of the PL band—from ~ 0.43 eV to ~ 0.50 eV—is a clear signature of a formation of donor states with an ensuing band filling effect, which confirms previous magneto-transport studies [33, 35]. This blue-shift saturates with increasing d_H . Finally, the integrated PL intensity increases with d_H , by more than one order of magnitude. Similar results are obtained for hydrogenations at $T_H=300$ °C, as well for a sample with a slightly higher N content ($x=0.0003$, not shown here).

In samples with increasing N content and exposed to the same hydrogenation doses and temperature ($T_H=250$ °C) as for the $x=0.0002$ sample shown in Fig. 1 (b), *no blue shift of the PL*

emission is observed. However, as shown in Fig. 2 (a), when the hydrogenation temperature is increased to $T_H=300$ °C, the PL peak intensity in a sample with $x=0.0015$ first increases by a factor of 4 ($d_H=1\times 10^{16}$ ions·cm⁻²), then it decreases severely and a broad band begins to appear underneath the emission of the as-grown sample, thus extending the sample PL up to ~ 0.65 eV for $d_H=10\times 10^{16}$ ions·cm⁻². At higher hydrogenation doses ($d_H=30\times 10^{16}$ ions·cm⁻²) this broad band dominates the spectrum (and extends to slightly higher energies). A similar behavior is observed for the $x=0.006$ sample. No shift of the PL emission is observed for $T_H=300$ °C but, as soon as the

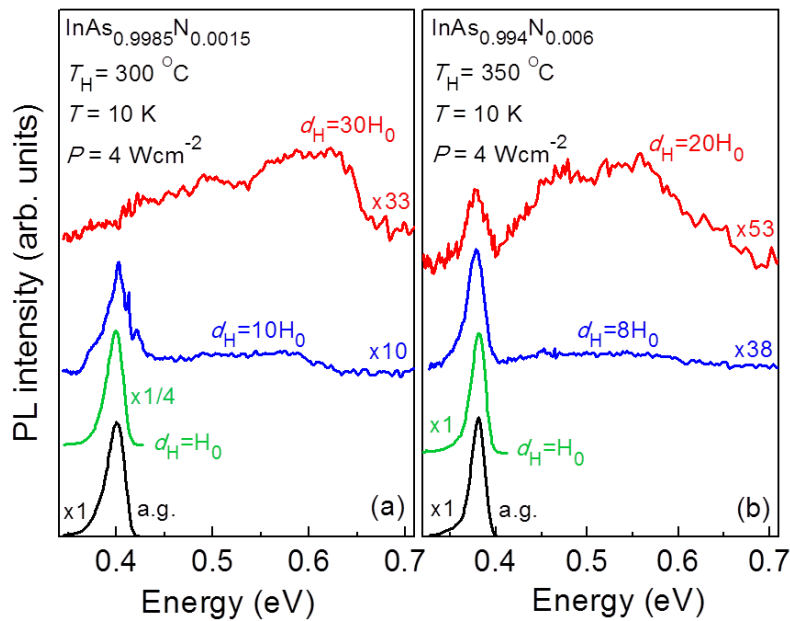


Figure 2. (color online) Peak normalized PL spectra taken at $T=10$ K ($P=4$ Wcm⁻²) for increasing doses of impinging H ions ($H_0=1\times 10^{16}$ ions·cm⁻²) in two 1 μ m-thick samples: (a) an InAs_{0.9985}N_{0.0015} sample irradiated at $T_H=300$ °C; (b) an InAs_{0.994}N_{0.006} sample irradiated at $T_H=350$ °C. Renormalization factors are indicated for each spectrum. (Power densities 20 to 30 times higher than those used for all other spectra have been used to obtain the PL spectra at the highest H doses, because of a severe decrease in the PL intensity). a.g. labels the as-grown samples.

hydrogenation temperature is raised to $T_H=350$ °C and the H dose to $d_H=8\times 10^{16}$ ions·cm⁻², a weak, broad band adds to that observed in the as-grown sample; see Fig. 2 (b). The strength of this band increases with H dose until it dominates the PL spectra for $d_H=20\times 10^{16}$ ions·cm⁻². It should be noticed, however, that these layers have thickness of ~ 1 μ m and for this high N content the sample has not been uniformly filled up with H atoms, even at the highest H dose: A residual emission

peak is observed at 0.38 eV, corresponding to the energy of the as-grown sample. Moreover, the high-energy band-edge is slightly lower than for the $x=0.0015$ sample; see Fig. 2 (a). Samples irradiated with even higher H doses could not be investigated because of the strong decrease in the PL signal, to almost below the detection limit. Therefore, evidence of band filling due to donors for N content $x=0.011$ could not be achieved for T_H up to 375 °C in these 1 μm -thick samples. Hydrogenations at higher temperatures have not been attempted in order to avoid donor complex dissociation, as it will be discussed in the following.

To summarize, the observation of an increase in carrier density requires higher hydrogenation temperatures and doses for increasing N contents. This suggests that a greater N-trap density should be counterbalanced by a greater diffusion length and H-dose, namely, the observation of a carrier-density increase does depend on the fraction of sample filled up with H atoms –and related donors. This assumption has been verified by irradiating thinner In(AsN) sample, 0.33 μm in

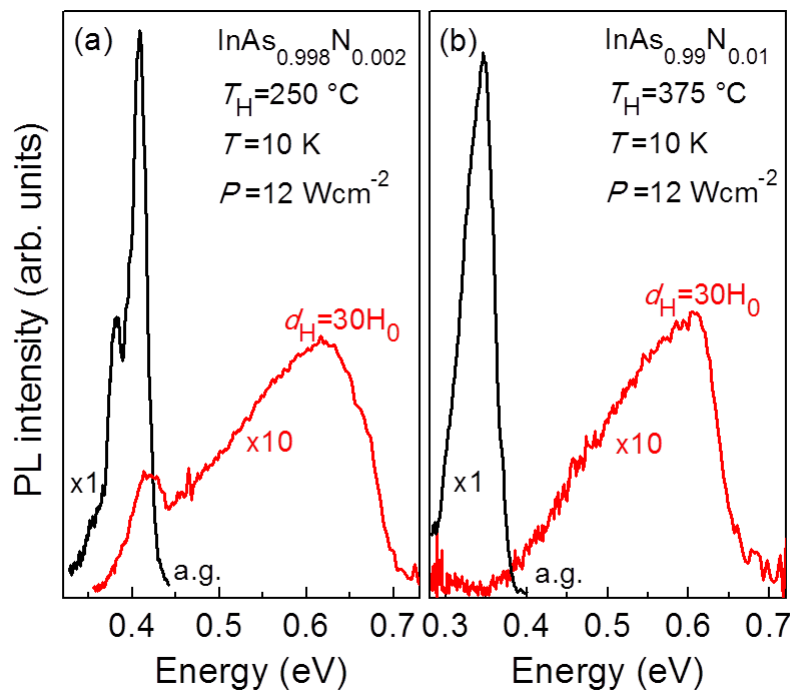


Figure 3. (color online) Peak normalized PL spectra taken at $T=10$ K ($P=12\text{Wcm}^{-2}$) for $d_H=30H_0$ ($H_0=1\times 10^{16}$ ions $\cdot\text{cm}^{-2}$) in two thin (0.33 μm thick) samples: (a) an $\text{InAs}_{0.998}\text{N}_{0.002}$ sample irradiated at $T_H= 250$ °C; (b) an $\text{InAs}_{0.99}\text{N}_{0.01}$ sample irradiated at $T_H= 375$ °C. Renormalization factors are indicated for each spectrum. a.g. labels the as-grown samples.

thickness, with H doses and at temperatures for which *no donor formation was inferred* from PL spectra in the 1 μm -thick samples. The PL spectra of two such 0.33 μm -thick samples containing N at $x=0.0002$ and 0.001 , and irradiated at $250\text{ }^\circ\text{C}$ with $d_{\text{H}}=30\times 10^{16}\text{ ions}\cdot\text{cm}^{-2}$ and $375\text{ }^\circ\text{C}$ with $d_{\text{H}}=30\times 10^{16}\text{ ions}\cdot\text{cm}^{-2}$, respectively, are shown in Fig. 3, together with the spectra of the as-grown samples. *In both samples, the PL spectra indicate an increase in the carrier concentration*, with a saturation of the Fermi energy at roughly the same value ($\sim 0.63\text{ eV}$) found in the 1 μm -thick samples, irrespective of the N content.

3.2. Secondary ion mass spectrometry

Photoluminescence results have been correlated with direct measurements of deuterium distribution profiles as obtained by SIMS in two pieces of a sample containing N at $x=0.0015$, one as grown and the other deuterated at $250\text{ }^\circ\text{C}$ or $300\text{ }^\circ\text{C}$, as shown in Fig. 4. In the sample deuterated at $250\text{ }^\circ\text{C}$, D atoms pervade roughly one third of the sample and no evidence of an increase in carrier concentration has been found; see PL spectra in the inset of panel (a). In the sample deuterated at $300\text{ }^\circ\text{C}$, more than two thirds of the sample is filled up with D atoms and the carrier density increases; see the inset of panel (b) and Fig. 2 (a). This provides direct evidence that the reliable detection of an increase in the carrier concentration using PL is possible only if a substantial fraction of the sample is filled up with D (H) atoms. We note that our earlier transport measurements in 1 μm -thick In(AsN) Hall bars hydrogenated at $T_{\text{H}}=250\text{ }^\circ\text{C}$, together with Raman measurements of the longitudinal-optical, LO, phonon-plasmon mode, [33] showed that the carrier concentration *actually* increases even in those samples, also hydrogenated at $T_{\text{H}}=250\text{ }^\circ\text{C}$, for which no carrier increase had been observed here in the PL spectra. For example, an $x=0.002$ (0.01) sample irradiated at $T_{\text{H}}=250\text{ }^\circ\text{C}$ with $d_{\text{H}}=4\times 10^{17}$

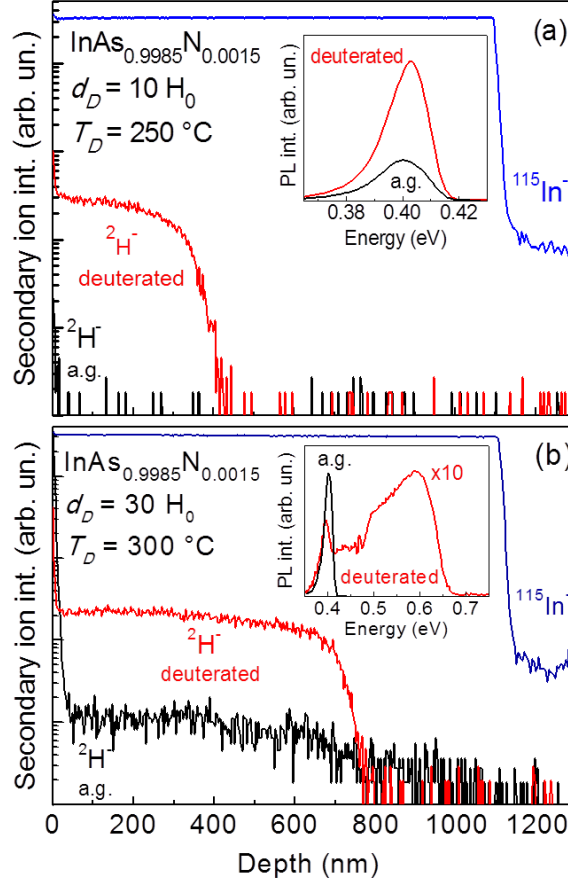


Figure 4. (color online) SIMS profile of D diffusion in In(AsN) samples with $x=0.0015$, as grown (black lines) and D-irradiated (red lines). The samples displayed in panel (a) were irradiated with a D dose $d_D = 10^{17}$ ions \cdot cm $^{-2}$ ($T_D = 250$ °C), while the samples shown in panel (b) were treated with a dose $d_D = 3 \times 10^{17}$ ions \cdot cm $^{-2}$ ($T_D = 300$ °C). The blue lines refer to the In profile, which determines the interface between the In(AsN) epilayer and the GaAs substrate. The insets show the PL spectra of the as grown (black lines) and deuterated (red lines) samples.

ions \cdot cm $^{-2}$, exhibited a carrier concentration of $n=2.5 \times 10^{18}$ - 4×10^{18} cm $^{-3}$ (0.5×10^{19} - 1.4×10^{19} cm $^{-3}$), as estimated from Hall effect or Shubnikov de Haas measurements, respectively. [33]

Finally, it should be pointed out that the N-free InAs energy gap is not recovered for any hydrogenation condition or N content, which is rather clear from the PL spectra of the $x=0.006$ sample hydrogenated at $T_H=350$ °C with $d_H=20 \times 10^{16}$ ions \cdot cm $^{-2}$: In that case, the as-grown and hydrogenated samples share the same threshold for PL emission; see Fig. 2 (b). Therefore, H does not neutralize the electronic activity of N in In(AsN), in contrast with findings in other dilute nitrides –i.e., Ga(AsN), Ga(PN), and (InGa)(AsN). [17, 22]

4. Discussion

4.1. Photoluminescence vs transport results

It has been outlined that magneto-transport and Raman scattering data seemingly disagree with the PL results found here in the same or similar thick samples. In particular, it has been shown that the optical detection of a carrier increase critically depends on the fraction of the sample filled up with D (or H) atoms. We speculate that whenever deuterium does not fill uniformly all or a major part of the sample –as in the case of the $x=0.0015$ sample hydrogenated at $T_H=250$ °C; see Fig. 4 (a)– a gradient develops in the concentration of D (or H) atoms and related donors. The leveling of the Fermi energy thus leads to a band bending and to the establishment of a built-in electric field in a more or less extended region below the sample surface where photo-generated carriers are rapidly separated. A subsurface “optically-dead layer” is thus established and carrier recombination strongly suppressed. However, this recombination is maintained, within the sample, in the region further away from the surface *where no sizable donor gradient is present* and the valence and conduction bands are flat. Transport measurements are dominated by the near-the-surface sample region with higher conductivity and more easily show a carrier increase, as supported by Raman measurements. [33] The optically-dead layer does not form when the sample is hydrogenated at high H doses and temperatures [as for the $x=0.0015$ sample hydrogenated at $T_H=300$ °C, panel (b) in Fig. 4] or when the same smaller H doses and temperatures are used for thinner (0.33 μm) samples. In these cases, samples are homogeneously filled up with H atoms and radiative recombination from an increased density of carriers is observed.

4.2. Nature of the H related donors

As regards the nature (and origin) of the H related donors, it cannot be due to irradiation damage –often resulting in the formation of vacancies, antisites, and interstitials acting as donors– [42] because the line-shape and intensity of the PL spectra of a number of In(AsN) samples do not

sizably change when they are irradiated with ^4He ions, which are heavier and much less chemically active than H ions. This effect is shown in Fig. 5 for an $x=0.0015$ sample irradiated at $T_{\text{H}}=300\text{ }^\circ\text{C}$ with a dose $d_{\text{He}}=3\times 10^{17}\text{ ions}\cdot\text{cm}^{-2}$ (namely, the conditions that in the case of H irradiation lead to a Fermi energy equal to 0.645 eV *and to a strong decrease in PL intensity*; see

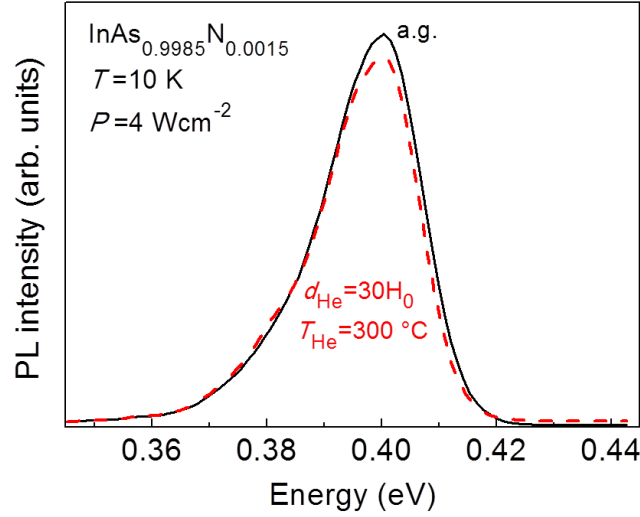


Figure 5. (color online) PL spectra taken at $T=10\text{ K}$ in two $1\mu\text{m}$ -thick $\text{InAs}_{0.9985}\text{N}_{0.0015}$ samples, one as-grown (black solid line) and the other irradiated with He ions (red dashed line) at the same temperature and dose of the hydrogenated sample shown in Fig. 2 (a).

Fig. 2 (a)). Neither can thermal effects account for the hydrogenation behavior reported in this paper: Only a factor of 2 increase, at most, in the PL efficiency has been observed in a few as-grown $x=0.0015$ and 0.01 samples, heated in vacuum at $250\text{ }^\circ\text{C}$ and $300\text{ }^\circ\text{C}$, respectively, for time intervals comparable to those used in the corresponding hydrogenations (not shown here). However, it should be mentioned that improvements in the PL emission intensity by factor of ~ 25 have been achieved by a *rapid thermal annealing* (30 s) of the sample performed *at much higher temperatures* (from $400\text{ }^\circ\text{C}$ to $550\text{ }^\circ\text{C}$). [43]

The microscopic nature of the H related donors is unveiled by Raman scattering data taken in two $x=0.01$ samples, one as grown and the other hydrogenated at $d_{\text{H}}=1\times 10^{18}\text{ ions}\cdot\text{cm}^{-2}$, and in a N-free sample. As it can be seen in Fig. 6 (a), for the hydrogenated (blue line) and virgin (red line) $\text{In}(\text{AsN})$ epilayers, the Raman peaks associated with the transverse (TO) and longitudinal (LO)

optical phonons, and their Raman second order, dominate the spectra at low frequency ($< 500 \text{ cm}^{-1}$). Besides, a broad Raman peak between the TO and the LO lines is clearly observed in both samples and attributed to a coupled LO phonon-plasmon L^- mode, as seen in n -type InAs [44] and In(AsN). [45] An additional broad peak, L^+ , emerges instead at high frequencies ($\sim 1200 \text{ cm}^{-1}$) and is observed only in hydrogenated In(AsN). We attribute the L^+ band to a coupled LO phonon-plasmon mode in the bulk epilayer due to the hydrogen-induced increase of the electron concentration. [33]

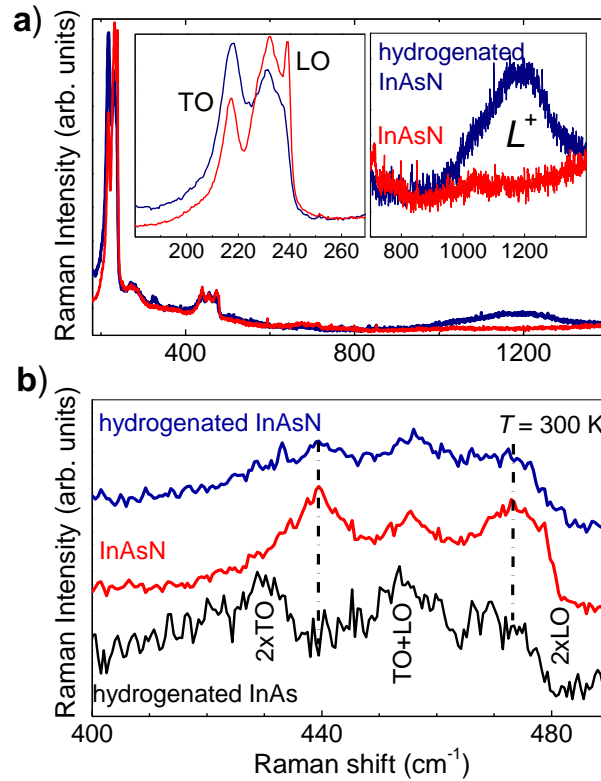


Figure 6. (Color online) a) Normalized Raman spectra of as-grown (red line) and hydrogenated (blue line) In(AsN) sample with $x=0.01$ at $T = 300 \text{ K}$. The insets show the same Raman spectra over selected frequency ranges. b) Zoom of the Raman spectra around the second order peaks. The spectrum for an hydrogenated InAs (black line) sample is included for comparison reasons. Vertical dashed lines indicate the positions of the In-N local mode (439 cm^{-1}) and isolated substitutional nitrogen mode (472 cm^{-1}) affected by hydrogenation. For clarity the spectra are shifted along the vertical axis. For all the hydrogenated epilayers, $T_H=250 \text{ }^\circ\text{C}$ and $d_H=100 \text{ H}_0=1 \times 10^{18} \text{ ions} \cdot \text{cm}^{-2}$.

We now focus on the Raman second order peaks shown in Fig. 6 (b) comparing hydrogenated (blue line) and virgin (red line) In(AsN) epilayers, as well as hydrogenated N-free InAs (black line). Two modes appear in the Raman spectra, at 439 cm^{-1} and 472 cm^{-1} , of the as-grown and of the hydrogenated In(AsN) sample. These modes are absent in the spectrum of the InAs sample hydrogenated at the same dose of the In(AsN) sample. This latter shows, instead, second harmonics of the LO and TO InAs phonon modes, as well as combination of these two modes (TO+LO), as indicated in the figure. The mode at around 472 cm^{-1} , which is almost overlapping the $2\times\text{LO}$ combination mode, has been attributed to a local vibrational mode due to isolated substitutional nitrogen, N_{As} . [46] A degenerate N_{As} local vibrational mode corresponding to the In-N bond energy was observed also near 438 cm^{-1} in Refs. 47 and 48. In In(AsN), hydrogenation partially restores the Raman spectrum of the N-free InAs sample, with a sizable quenching of the mode at 439 cm^{-1} and an almost full quenching of the mode at 472 cm^{-1} , thus showing that In-N local bonds break upon hydrogenation and that H-N complexes form. Similar results have also been obtained on a $x=0.002$ In(AsN) sample. However, further Raman measurements in other samples are required for a more robust statement.

We speculate that the donor complex involved is due to H in a bond center or a N-antibonding stable site, as theoretically predicted [49] and experimentally reported in the case of InN, [10] (InGa)N – where four-H complexes are also predicted and shown to form and act as donors as well–, [11] and GaN [9, 12] – where H has an amphoteric behavior.

4.3. Fermi stabilization energy

We now discuss in some detail the dependence of the energy gap (E_g), Fermi energy (E_F), and carrier concentration (n) on H dose and N content. These values have been estimated from simulations of the PL line-shapes carried out in the framework of a semi-relativistic two-band model [50] according to which the energy dispersion for the conduction electrons is given by [51]

$$E(\vec{k}) = \sqrt{\left(\frac{E_g}{2}\right)^2 + E_g \frac{\hbar^2 k^2}{2m_e^*}} - \frac{E_g}{2}. \quad (1)$$

$m_e^* = 0.025m_0$ is the electron effective mass at the conduction band edge in InAs [52], m_0 is the electron rest mass. For each spectrum, the line-shape was simulated using the following expression:

$$I(E) = A \int g(E') f(E') G(E - E') dE', \quad (2)$$

where A is a constant, $g(E) = \frac{m_e^* \sqrt{2m_e^* E}}{\pi^2 \hbar^3} \left(1 + \frac{2E}{E_g}\right) \sqrt{1 + \frac{E}{E_g}}$ is the density of states calculated according to the dispersion given by Eq. (1), $f(E)$ is the Fermi-Dirac probability function, and $G(E)$ is a Gaussian function accounting for a broadening of the electronic states. [53] Finally, the

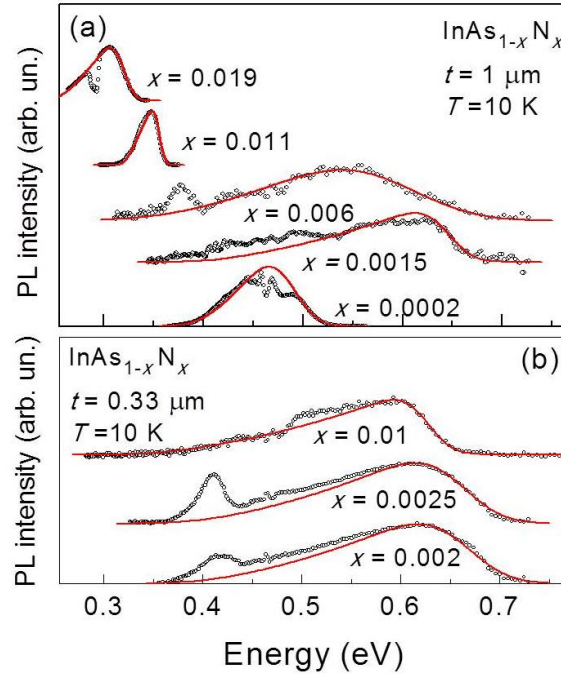


Figure 7. (color online) (a) PL spectra for all the investigated thick ($\sim 1.0 \mu\text{m}$) samples, together with their best simulations as obtained by Eq. 2, see text. (b) PL spectra for all the investigated thin ($0.33 \mu\text{m}$) samples, together with their best simulations as obtained by Eq. 2; see text. All spectra have been taken in samples irradiated with hydrogen at conditions providing the maximum increase in carrier density.

electron density was calculated as $n = \int_{E_g}^{E_F} g(E)f(E)dE$, where the values of E_g and E_F are those that give the best agreement between the experimental data and the simulated PL spectra. The simulations of the PL spectra are shown in Figs. 7 (a) and 7 (b) for all the investigated thick and thin samples, respectively. All spectra have been taken for samples where conditions of hydrogen irradiation provided the highest increase in carrier density. Some dips in the spectra, as for the $x=0.019$ sample, are due to atmospheric absorption. Full hydrogenation is never achieved in the whole sample depth, even in the thin samples, as shown by the persistence of a band at 0.4 eV. Therefore, a hydrogen gradient is established along the sample and the PL spectra are largely broadened. The estimated values of E_g , E_F , and n of samples showing the highest increase in carrier density as obtained by the spectra simulations displayed in Fig. 7 are given in Table I together with the corresponding values of N content (x), thickness (t), and hydrogenation conditions (d_H and T_H) of the investigated samples. Carrier concentrations as derived from magneto-transport (Hall and Shubnikov de Haas effect) measurements [33, 35] are close to those obtained here from the simulation of the PL emission line-shape.

Table I. Values of energy gap (E_g), Fermi energy (E_F), and carrier density (n) of $\text{InAs}_{1-x}\text{N}_x$ samples as obtained from the simulations shown in Fig. 7 for the samples exhibiting the highest increases in carrier density. N content (x), sample thickness (t), and hydrogenation conditions (d_H and T_H) are also given for each sample. $H_0=10^{16}$ ions·cm⁻².

N content x	Thickness t (μm)	H dose d_H (H_0)	Hydrogenation temperature T_H ($^{\circ}\text{C}$)	Energy gap E_g (eV)	Fermi energy E_F (eV)	Carrier concentration n (10^{17}cm^{-3})
0.0002	1	30	250	0.40	0.49	6.8
0.0015	1	30	300	0.40	0.64	44
0.0060	1	20	350	0.35	0.60	49
0.011	1	1	250	0.32	0.36	1.4
0.019	1	1	300	0.25	0.32	4.3
0.002	0.33	30	250	0.39	0.67	58
0.0025	0.33	30	250	0.38	0.66	59
0.010	0.33	30	375	0.34	0.63	67

From the PL studies we find that the electron concentration increases with N concentration (for a fixed d_H) and H dose (for a fixed N concentration, not shown here) –thus supporting the formation of H-N donor complexes–, as well as with increasing hydrogenation temperature or decreasing sample thickness. More interestingly, the Fermi energy as estimated by PL data tends to saturate (near 0.67 eV, namely, 0.25 eV above the conduction band minimum, CBM) for decreasing sample thickness (0.33 μm) and increasing N content. This saturation suggests that a stabilized Fermi energy, E_{FS} , [36, 54] is achieved in In(AsN). In fact, acceptors and donors related to native defects would have the same formation energy and compensate each other for $E_F = E_{FS}$, with an ensuing saturation of carrier density. A Fermi stabilization energy also accounts for the attainment, in the 0.33 μm -thick $\text{InAs}_{0.99}\text{N}_{0.01}$ sample, of a maximum carrier concentration ($\sim 6.7 \times 10^{18} \text{ cm}^{-3}$) that is at least one order of magnitude smaller than both the N and H densities. In this sample, the N density is equal to $1.8 \times 10^{20} \text{ cm}^{-3}$, the H density to $1.1 \times 10^{20} \text{ cm}^{-3}$ –as estimated from the impinging dose of H ions ($3 \times 10^{17} \text{ ions}\cdot\text{cm}^{-2}$), the sample thickness (0.33 μm), and the reflection coefficient of low-energy H ions [$1.2 \pm 0.4\%$ in the case of D impinging on Ga(AsN)]. [55] A Fermi stabilization level 0.25 eV above the InAs CBM can also account for the electron accumulation-layer usually found at the InAs surface. [37, 56, 57] Moreover, E_{FS} would be ~ 4.65 eV (4.8 eV) below the vacuum level, for InAs electron affinity of 4.9 eV (5.06 eV) [58, 59]. These values imply that the amphoteric defect model with a “universal” value of E_{FS} [54], which has been found to hold for wide gap semiconductors, equally applies to narrow gap semiconductors: A Fermi stabilization energy of 4.9 eV below the vacuum level has indeed been determined by measurements of the electron concentrations in InN and In-rich (InGa)N (irradiated with 1 MeV electrons, 2 MeV protons, and 2 MeV $^4\text{He}^+$) [42] and of the hole concentration in SnTe (irradiated with MeV Ne^+ ions). [60]

4.4. Absence of H related donors in N-free InAs

Finally, the transition from defect passivation in InAs to donor formation in In(AsN) can be accounted for on the grounds of the predicted H effects in (InGa)(AsN), [18] provided that the H $\varepsilon^{+/-}$ transition level lies *just below* the InAs CBM. In this case, H would have an amphoteric behavior and act as a donor or acceptor depending on the *p*- or *n*-type material doping, respectively, thus passivating any type of dominant non radiative defects, [18] as observed in InAs; see Fig. 1 (a). As soon as N is introduced in the host InAs lattice, the InAs band gap decreases and the CBM moves down toward the valence band maximum. If the H transition level $\varepsilon^{+/-}$ is *just below* the InAs CBM, in In(AsN) it moves into the conduction band and H atoms can only act as donors, most likely in complexes with N atoms –as suggested by Raman scattering. The carrier concentration would then increase and, as soon as the Fermi energy reaches the Fermi stabilization energy, H atoms would only be present in inactive states, *e.g.* interstitial H₂ molecules, in agreement with present results in hydrogenated In(AsN). It is interesting to note here that it has been recently predicted [13] that the surface transition level of H adsorbed on the InAs surface lies *just above* CBM, in contrast to the case of InP, GaAs, and possibly GaSb, where it lies well below CBM, as in the bulk.

4.5. Stability of H related donors

The aforementioned increase in carrier concentration (by orders of magnitude), with no significant effect on carrier mobility, [33] could be exploited for technological applications provided these increases are thermally stable. The activation energy for the dissociation of the H-N donor complexes has been investigated here by exposing different In(AsN) samples to cycles of isochronal annealings and determining their carrier density with different techniques. A 0.33 μm -thick InAs_{0.99}N_{0.01} sample, irradiated with $d_{\text{H}}=4\times 10^{17}$ ions·cm⁻² at $T_{\text{H}}=375$ °C and exposed to 4 hr annealings, has been studied by PL measurements. A 1 μm -thick InAs_{0.9985}N_{0.0015} sample, irradiated with $d_{\text{H}}=1\times 10^{16}$ ions·cm⁻² at $T_{\text{H}}=300$ °C and exposed to 1 hr annealings in a furnace in a continuous Ar flow, has been also investigated in parallel by Hall effect measurements. The PL

spectra taken at low temperature in the thin (0.33 μm) $x=0.01$ sample are shown by full dots in Fig. 8 for various annealing temperatures, together with the spectrum of the as-grown sample for comparison purposes. A rapid inspection of these spectra indicates that the band filling decreases for increasing annealing temperature. However, the line-shape of the as-grown sample is never fully recovered, even at $T_a=898$ K. A detailed data analysis has been performed by simulating the

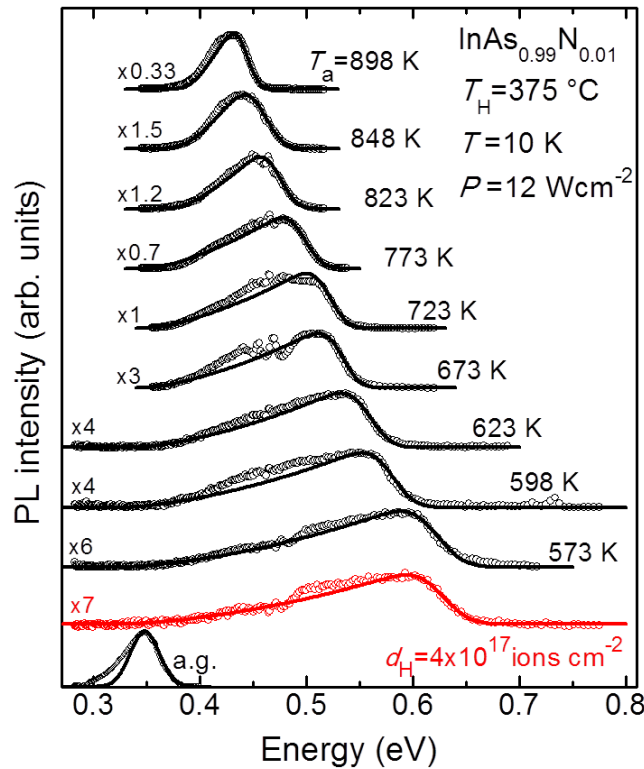


Figure 8. (color online) PL spectra (full dots) of an $\text{In}(\text{AsN})$ sample with $x=0.01$ hydrogenated at $d_H=4\times 10^{17}$ ions $\cdot\text{cm}^{-2}$ and $T_H=375$ °C and exposed to 4 hours annealing cycles at increasing temperatures T_a . The PL spectrum taken from the same as-grown (a.g.) sample is also shown. Solid lines are simulations of the data by the theoretical model discussed in the text.

spectra (full lines in the figure) using the previously introduced theoretical model so that the band gap and Fermi energy could be estimated at each annealing temperature. Some minor misfits may be due to approximations in the density of states and/or the application of the same system response to all data, when ambient humidity was in fact changing from day to day. The values of the carrier density thus obtained for both the thin $x=0.01$ and thick $x=0.0015$ sample are shown in Fig. 9 as a

function of annealing temperature, together with the values of E_g in the thin sample. The band gap energy increases from the value it has in the non annealed sample as soon as the annealing temperature exceeds 600 K and progressively tends toward the value in InAs, but without reaching it; see panel (a). This blue-shift of the energy gap indicates that N atoms desorb from the sample (a desorption of As atoms, on the contrary, would decrease E_g by increasing the relative N content). The carrier density decreases with T_a in the thick $x=0.0015$ sample sooner (at ≈ 500 K) than in the thin $x=0.01$ sample (at ≈ 600 K), see panel (b), suggesting that different donor complexes might appear in the two samples, and/or that the dynamics of H trapping and detrapping depends on the N content in the sample and/or the thickness of the H-penetrated layer.

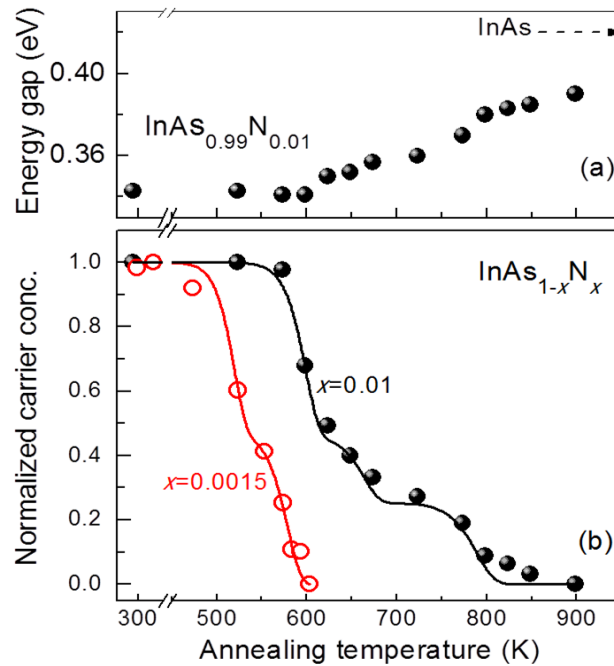


Figure 9. (color online) (a) Values of the energy gap estimated from the PL spectra of a hydrogenated $\text{InAs}_{0.99}\text{N}_{0.01}$ sample as a function of annealing temperature, T_a . A dashed arrow points to the value of the InAs energy gap (at 4 K). (b) Values of the carrier concentration (full dots), n —estimated for the same $\text{InAs}_{0.99}\text{N}_{0.01}$ sample and normalized to the value $6.8 \times 10^{18} \text{ cm}^{-3}$ before the annealing cycles— vs T_a . In the same panel (b), the values of n —estimated by Hall Effect measurements (open circles) in a hydrogenated $\text{InAs}_{0.9985}\text{N}_{0.0015}$ sample and normalized to the value $4.5 \times 10^{18} \text{ cm}^{-3}$ before the annealing cycles— are shown vs T_a . Lines are theoretical fits of Eq. 3 to the data, as explained in the text.

An Arrhenius-like formula [10]

$$n_d(T) = \sum_i n_{0i} e^{-v_{ai}t} e^{(-E_{ai}/k_B T)} + c \quad (3)$$

has been then fitted to the two sets of data, as shown by full lines in Fig. 9 (b). In the above equation, c is a constant, v_{ai} are attempt frequencies of H related complexes, n_{0i} the initial defect populations, and E_{ai} are activation energies for the restoration of the donor complexes created upon hydrogenation. A value typical of H-related complexes in InN (3400 cm^{-1} ; see Ref. 10) has been taken for both the attempt frequencies. In both thin and thick samples, the passivation of more than a single defect is required to obtain a good fit to the data, as shown in Table II. Therein, the activation energies for H desorption found in InN [10] are also included. In the case of thin $x=0.01$ (thick $x=0.0015$) samples, the deactivation of three (two) different defects is required in order to get a good fit to the

Table II. Best-fit values of the initial defect populations (n_{0i} , in units $n_0=10^{18} \text{ cm}^{-3}$) and activation energies (E_{ai}) for the restoration of the In(AsN) non-radiative defects passivated by H as determined by the thermal annealing studies shown in Fig. 9. c is the defect population after all the annealings; see Eq. 3. The values obtained in hydrogenated InN (see Ref. 10) have also been reported for comparison purposes.

Sample	n_{01} (n_0)	E_{a1} (eV)	n_{02} (n_0)	E_{a2} (eV)	n_{03} (n_0)	E_{a3} (eV)	c (n_0)
InAs _{0.9985} N _{0.0015}	1.6	1.8±0.1	1.4	2.0±0.1			1.4
InAs _{0.99} N _{0.01}	3.4	2.2±0.1	1.3	2.4±0.1	1.6	2.9±0.1	0.4
InN [10]	0.45	1.97±0.06	0.38	2.18±0.07			1.0

data. Although a single activation energy was required to fit H desorption in hydrogenated GaP_{0.0994}N_{0.006}, [61] and two activation energies in InN, [10] a good fit of annealing data in other hydrogenated dilute nitrides was obtained only by assuming a Gaussian distribution of the deactivation energies with a mean value $\langle E_a \rangle = 2.2 \text{ eV}$ and standard deviation σ of $\pm 0.35 \text{ eV}$ in a GaAs_{0.97}N_{0.03} sample [62] and $2.28 \pm 0.26 \text{ eV}$, in a In_{0.34}Ga_{0.66}As_{0.993}N_{0.007} sample. [63] Moreover,

the mean value of the activation energy $\langle E_a \rangle$ in (InGa)(AsN) increases from 2.26 eV to 2.38 eV for a N concentration increasing from $x=0.007$ to $x=0.052$. [59] Therein, the increase in the activation energy with N content was attributed to an increasing fraction of multi-N complexes (couples, triplets, etc) capable of forming stronger bonds with H atoms, as may be the case here, too.

More annealing steps would be required for a precise determination of the activation energies involved in the H desorption process. However, some conclusions can be drawn already from present annealing results. First, donor formation is stable up to at least 500 K; second, several types of H-related donors may form in In(AsN), with different activation energies for H; third, the sample stoichiometry starts changing for annealing temperatures greater than 600 K. The results obtained in this work provide a valuable information that could enable band gap engineering of In(AsN)-based devices relying on the tuning of the donor concentration by hydrogen —either through a suitable metallic mask impeding H-implantation into specific areas of the sample or by profiling the sample with localized thermal annealing by an intense laser beam. [64, 65]

5. Conclusions

In summary, photoluminescence measurements in a number of In(AsN) samples for increasing hydrogen doses and/or hydrogenation temperatures have shown that the sample's native carrier concentration increases *provided that a few N atoms substitute As atoms*. This H-induced effect is ruled by a competition between an initial H passivation of native defects followed by a H-induced creation of defects (at a rate increasing with N content and H dose) and formation of H-N donor complexes (for suitable hydrogenation doses and temperatures). The increase in carrier concentration stops as soon as the Fermi energy reaches the Fermi stabilization energy, 4.7 ± 0.1 eV below the vacuum level. A hydrogen transition level $\epsilon^{+/-}$ just below the bottom of the InAs conduction band would explain the insurgence of H-N donor complexes as soon as N atoms substitute just 0.02% of As atoms. Raman scattering measurements support the formation of H-N donor complexes, which are thermally stable up to ~ 500 K. Annealing at temperatures higher than

600 K favors a change in the material stoichiometry with an ensuing increase in the band gap energy. A development of novel devices based on an in-plane engineering of the electrical conductivity of In(AsN) with the help of post-growth hydrogenation may emerge in the foreseeable future.

ACKNOWLEDGEMENTS

The authors acknowledge M. De Luca (Sapienza University of Rome) for preliminary measurements on hydrogenated In(AsN). M. C. and A. P. acknowledge funding from Sapienza University of Rome, through Fondi Ateneo 2012 and 2013, respectively.

FIGURE CAPTIONS

Figure 1. (color online) Peak normalized PL spectra taken at $T=10$ K ($P=4$ Wcm⁻²) for increasing doses of impinging H ions ($H_0=1\times 10^{16}$ ions·cm⁻²) in two 1 μ m-thick samples: (a) InAs, and (b) an InAs_{0.9998}N_{0.0002} sample, both irradiated at $T_H=250$ °C. The dips on the high energy side of the PL spectra are due to atmospheric air absorption. Renormalization factors are indicated for each spectrum. a.g. labels the as-grown samples.

Figure 2. (color online) Peak normalized PL spectra taken at $T=10$ K ($P=4$ Wcm⁻²) for increasing doses of impinging H ions ($H_0=1\times 10^{16}$ ions·cm⁻²) in two 1 μ m-thick samples: (a) an InAs_{0.9985}N_{0.0015} sample irradiated at $T_H=300$ °C; (b) an InAs_{0.994}N_{0.006} sample irradiated at $T_H=350$ °C. Renormalization factors are indicated for each spectrum. (Power densities 20 to 30 times higher than those used for all other spectra have been used to obtain the PL spectra at the highest H doses, because of a severe decrease in the PL intensity). a.g. labels the as-grown samples.

Figure 3. (color online) Peak normalized PL spectra taken at $T=10$ K ($P=12$ Wcm⁻²) for $d_H=30H_0$ ($H_0=1\times 10^{16}$ ions·cm⁻²) in two thin (0.33 μ m thick) samples: (a) an InAs_{0.998}N_{0.002} sample irradiated at $T_H=250$ °C; (b) an InAs_{0.99}N_{0.01} sample irradiated at $T_H=375$ °C. Renormalization factors are indicated for each spectrum. a.g. labels the as-grown samples.

Figure 4. (color online) SIMS profile of D diffusion in In(AsN) samples with $x=0.0015$, as grown (black lines) and D-irradiated (red lines). The samples displayed in panel (a) were irradiated with a D dose $d_D=10^{17}$ ions·cm⁻² ($T_D=250$ °C), while the samples shown in panel (b) were treated with a dose $d_D=3\times 10^{17}$ ions·cm⁻² ($T_D=300$ °C). The blue lines refer to the In profile, which determines

the interface between the In(AsN) epilayer and the GaAs substrate. The insets show the PL spectra of the as grown (black lines) and deuterated (red lines) samples.

Figure 5. (color online) PL spectra taken at $T=10$ K in two $1\mu\text{m}$ -thick $\text{InAs}_{0.0985}\text{N}_{0.0015}$ samples, one as-grown (black solid line) and the other irradiated with He ions (red dashed line) at the same temperature and dose of the hydrogenated sample shown in Fig. 2 (a).

Figure 6. (Color online) a) Normalized Raman spectra of as-grown (red line) and hydrogenated (blue line) In(AsN) sample with $x=0.01$ at $T = 300$ K. The insets show the same Raman spectra over selected frequency ranges. b) Zoom of the Raman spectra around the second order peaks. The spectrum for an hydrogenated InAs (black line) sample is included for comparison reasons. Vertical dashed lines indicate the positions of the In-N local mode (439 cm^{-1}) and isolated substitutional nitrogen mode (472 cm^{-1}) affected by hydrogenation. For clarity the spectra are shifted along the vertical axis. For all the hydrogenated epilayers, $T_{\text{H}}=250\text{ }^{\circ}\text{C}$ and $d_{\text{H}}=100\text{ H}_0=1\times 10^{18}\text{ ions}\cdot\text{cm}^{-2}$.

Figure 7. (color online) (a) PL spectra for all the investigated thick ($\sim 1.0\text{ }\mu\text{m}$) samples, together with their best simulations as obtained by Eq. 2, see text. (b) PL spectra for all the investigated thin ($0.33\text{ }\mu\text{m}$) samples, together with their best simulations as obtained by Eq. 2; see text. All spectra have been taken in samples irradiated with hydrogen at conditions providing the maximum increase in carrier density.

Figure 8. (color online) PL spectra (full dots) of an In(AsN) sample with $x=0.01$ hydrogenated at $d_{\text{H}}=4\times 10^{17}\text{ ions}\cdot\text{cm}^{-2}$ and $T_{\text{H}}=375\text{ }^{\circ}\text{C}$ and exposed to 4 hours annealing cycles at increasing

temperatures T_a . The PL spectrum taken from the same as-grown (a.g.) sample is also shown. Solid lines are simulations of the data by the theoretical model discussed in the text.

Figure 9. (color online) (a) Values of the energy gap estimated from the PL spectra of a hydrogenated $\text{InAs}_{0.99}\text{N}_{0.01}$ sample as a function of annealing temperature, T_a . A dashed arrow points to the value of the InAs energy gap (at 4 K). (b) Values of the carrier concentration (full dots), n –estimated for the same $\text{InAs}_{0.99}\text{N}_{0.01}$ sample and normalized to the value $6.8 \times 10^{18} \text{ cm}^{-3}$ before the annealing cycles– vs T_a . In the same panel (b), the values of n –estimated by Hall Effect measurements (open circles) in a hydrogenated $\text{InAs}_{0.9985}\text{N}_{0.0015}$ sample and normalized to the value $4.5 \times 10^{18} \text{ cm}^{-3}$ before the annealing cycles– are shown vs T_a . Lines are theoretical fits of Eq. 3 to the data, as explained in the text.

TABLE CAPTIONS

Table I. Values of energy gap (E_g), Fermi energy (E_F), and carrier density (n) of $\text{InAs}_{1-x}\text{N}_x$ samples as obtained from the simulations shown in Fig. 7 for the samples exhibiting the highest increases in carrier density. N content (x), sample thickness (t), and hydrogenation conditions (d_H and T_H) are also given for each sample. $H_0=10^{16}$ ions·cm⁻².

Table II. Best-fit values of the initial defect populations (n_{0i} , in units $n_0=10^{18}$ cm⁻³) and activation energies (E_{ai}) for the restoration of the In(AsN) non-radiative defects passivated by H as determined by the thermal annealing studies shown in Fig. 9. c is the defect population after all the annealings; see Eq. 3. The values obtained in hydrogenated InN (see Ref. 10) have also been reported for comparison purposes.

REFERENCES

- [1] Ren F 1994 *Mater. Sci. Forum* **148-149** 141
- [2] Pankove Jacques I and Johnson Noble M 1991 *Hydrogen in semiconductors (Semiconductors and semimetals vol. 34)* (Boston: Academic Press); Nickel N H 1999 *Hydrogen in semiconductors II (Semiconductors and semimetals vol. 61)* (Boston: Academic Press)
- [3] Pearton S J, Corbett J W and Stavola M 1992 *Hydrogen in Crystalline Semiconductors (Springer Series in Materials Science vol. 16)* (Berlin: Springer Verlag) - ISBN: 3-540-55491-2
- [4] Elias D C *et al.* 2009 *Science* **323** 610
- [5] Teukam Z *et al.* 2003 *Nature Mater.* **2** 482
- [6] Goennenwein S T B, Wassner T A, Huebl H, Brandt M S, Philipp J B, Opel M, Gross R, Koeder A, Schoch W and Waag A 2004 *Phys. Rev. Lett.* **92** 227202
- [7] Kilic C and Zunger A 2002 *Appl. Phys. Lett.* **81** 73
- [8] Van de Walle C G and Neugebauer J 2003 *Nature* **423** 626
- [9] Limpijumnong S and Van de Walle C G 2001 *phys. stat. sol. B* **228** 303
- [10] Pettinari G *et al.* 2008 *Phys. Rev. B* **77** 125207; and references therein
- [11] De Luca M *et al.* 2012 *Phys. Rev. B* **86** 201202
- [12] Myers S M, Wright A F, Petersen G A, Seager C H, Wampler W R, Crawford M H and Han J 2000 *J. Appl. Phys.* **88** 4676
- [13] Castleton C W M, Höglund A, Göthelid M, Qian M C and Mirbt S 2013 *Phys. Rev. B* **88** 045319
- [14] O'Reilly E P, Lindsay A, Klar P J, Polimeni A and Capizzi M 2009 *Semicond. Sci. Technol.* **24** 033001; and references therein
- [15] Buyanova I A and Chen W M 2004 *Physics and Applications of Dilute Nitrides* vol. 21, (New York: Taylor & Francis) - ISBN: 1-59169-019-6
- [16] Henini M 2005 *Dilute Nitride Semiconductors* (Amsterdam: Elsevier); Erol A 2008 *Dilute III-V Nitride Semiconductor and Material Systems (Springer Series in Materials Science vol. 105)* (Berlin: Springer) - ISBN: 0-08-044502-0
- [17] Ciatto G 2015 *Hydrogenated Dilute Nitride Semiconductors - Theory, Properties and Applications* (Singapore, Pan Stanford Publishing)
- [18] Janotti A, Zhang S B, Wei Su-Huai and Van de Walle C G 2002 *Phys. Rev. Lett.* **89** 086403
- [19] Fowler W B, Martin K R, Washer K and Stavola M 2005 *Phys. Rev. B* **72** 035208
- [20] Du M-H, Limpijumnong S and Zhang S B 2005 *Phys. Rev. B* **72** 073202

-
- [21] Wen L, Stavola M, Fowler W B, Trotta R, Polimeni A, Capizzi M, Bisognin G, Berti M, Rubini S and Martelli F 2012 *Phys. Rev. B* **86** 085206
- [22] Trotta R, Polimeni A and Capizzi M 2012 *Adv. Funct Mater.* (Feature Article) **22** 1782; and references therein
- [23] Birindelli S, Felici M, Wildmann J S, Polimeni A, Capizzi M, Gerardino A, Rubini S, Martelli F, Rastelli A and Trotta R 2014 *Nano Lett.* **14** 1275
- [24] De la Mare M, Zhuang Q, Krier A, Patanè A and Dhar S 2009 *Appl. Phys. Lett.* **95** 031110
- [25] Sandall I C, Bastiman F, White B, Richards R, Mendes D, David J P R and Tan C H 2014 *Appl. Phys. Lett.* **104** 171109
- [26] Kozlova N V, Mori N, Makarovskiy O, Eaves L, Zhuang Q D, Krier A and Patanè A 2012 *Nature Comm.* **3** 1097; and references therein.
- [27] Wang J S, Lin H H, Song L W and Chen G R 2001 *J. Vac. Sci. Technol. B* **19** 202
- [28] Veal T D, Piper L F J, Jefferson P H, Mahboob I, Mc Conville C F, Merrick M, Hose T J C, Murdin B N and Hopkinson M 2005 *Appl. Phys. Lett.* **87** 182114
- [29] Ruiz A, Gonzallez L, Mazuelas A and Briones F 1989 *Appl. Phys. A* **49** 543
- [30] Makarovskiy O, Feu W H M, Patanè A, Eaves L, Zhuang Q D, Krier A, Beanland R and Airey R 2011 *Appl. Phys. Lett.* **96** 052115
- [31] Katkov A V, Wang C C, Chi J Y, Cheng C and Gutakovskii A K 2011 *J. Vac. Sci. Technol. B* **29** 03C127
- [32] Polimeni A, Marangio D, Capizzi M, Frova A and Martelli F 1994 *Appl. Phys. Lett.* **65** 1254
- [33] Kozlova N V, Pettinari G, Makarovskiy O, Mori N, Polimeni A, Capizzi M, Zhuang Q D, Krier A and Patanè A 2013 *Phys. Rev. B* **87** 165207
- [34] Theys B, Lusson A, Chevallier J, Grattepain C, Kalem S and Stutzman M J 1991 *J. Appl. Phys.* **70** 1461
- [35] Velichko AV, Patanè A, Capizzi M, Sandall I C, Giubertoni D, Makarovskiy O, Polimeni A, Krier A, Zhuang Q and Tan C H 2015 *Appl. Phys. Lett.* **106** 022111
- [36] Walukiewicz W 1988 *Phys. Rev. B* **37** 4760; and references therein.
- [37] Wang P D, Holmes S N, Le Tan, Straddling R A, Ferguson T and de Oliveira A G 1992 *Semicond. Sci. Technol.* **7** 767
- [38] Shan W, Walukiewicz W, Ager J W III, Haller E E, Geisz J F, Friedman D J, Olson J M and Kurtz S R 1999 *Phys. Rev. Lett.* **82** 1221
- [39] Vurgaftman I, Meyer J and Ram-Mohan L 2001 *J. Appl. Phys.* **89** 5815

-
- [40] Zhuang Q, Godenir A, Krier A, Lai K and Haywood S 2008 *J. Appl. Phys.* **103** 063520
- [41] de la Mare M, Zhuang Q, Patanè A and Krier A 2012 *J. Phys. D: Appl. Phys.* **45** 395103
- [42] Li S X, Yu K M, Wu J, Jones R E, Walukiewicz W, Ager J W III, Shan W, Haller E E, Lu Hai and Schaff William J 2005 *Phys. Rev. B* **71**, 161201 (R)
- [43] Kesaria M, Birindelli S, Velichko A V, Zhuang Q D, Patanè A, Capizzi M and Krier A 2015 *Infrared Phys. & Technol.* **68** 138
- [44] Li Y B, Ferguson I T, Stradling R A and Zallen R 1992 *Semicond. Sci. Technol.* **7** 1149
- [45] Ibáñez J, Oliva R, De la Mare M, Schmidbauer M, Hernández S, Pellegrino P, Scurr D J, Cuscó R, Artús L, Shafi M, Mari R H, Henini M, Zhuang Q, Godenir A and Krier A 2010 *J. Appl. Phys.* **108** 103504
- [46] Alt H Ch, Egorov A Yu, Riechert H, Meyer J D and Wiedemann B 2011 *Physica B* **308-310** 877
- [47] Devki N Talwar, Tzuen-Rong Yang, Hao Hsiung Lin and Zhe Chuan Feng 2013 *Appl. Phys. Lett.* **102** 052110
- [48] Wagner J, Köhler K, Ganser P and Maier M 2005 *Appl. Phys. Lett.* **87** 051913
- [49] Van de Walle C G and Neugebauer J 2004 *J. Appl. Phys.* **95** 3581; and references therein
- [50] Kane E O 1957 *J. Phys. Chem. Solids* **1** 249
- [51] Zawadzki W, Klahn S and Merkt U 1985 *Phys. Rev. Lett.* **55** 983
- [52] Drachenko O, Patanè A, Kozlova N V, Zhuang Q D, Krier A, Eaves L and Helm H 2011 *Appl. Phys. Lett.* **98** 162109
- [53] Grilli E, Guzzi M, Zamboni R and Pavesi L 1992 *Phys. Rev. B* **45** 1638
- [54] Walukiewicz W 1989 *Appl. Phys. Lett.* **54** 2094
- [55] Berti M *et al.* 2007 *Phys. Rev. B* **76** 205323
- [56] Olsson L Ö, Andersson C B M, Håkansson M C, Kanski J, Ilver L and Karlsson U O 1996 *Phys. Rev. Lett.* **76** 3626
- [57] Weber J R, Janotti A and Van de Walle G C 2010 *Appl. Phys. Lett.* **97** 192106
- [58] Milnes A G and Feucht D L 1972 *Heterojunctions and metal-insulator transitions* (New York: Academic)
- [59] Adachi Sadao 2004 *Handbook on physical properties of semiconductors* vol. 2 (III-V Compound semiconductors) (Norwell, Ma, USA: Kluwer Academic Publishers).
- [60] Nishitani Junichi, Detert Douglas, Beeman Jeffrey, Yu Kin Man and Walukiewicz Wladek 2014 *Appl. Phys. Express* **7** 091201

-
- [61] Polimeni A, Bissiri M, Felici M, Capizzi M, Buyanova I A, Chen W M, Xin H P and Tu C W 2003 *Phys. Rev. B* **67** 201303
- [62] Bissiri M, Baldassarri Höger von Högersthal G, Polimeni A, Capizzi M, Gollub D, Fischer M, Reinhardt M and Forchel A 2002 *Phys. Rev. B* **66** 033311
- [63] Polimeni A *et al.* 2001 *Physica B* **308-310** 850
- [64] Trotta *et al.* 2011 *Adv. Mater.* **23** 2706
- [65] Balakrishnan N *et al.* 2012 *Phys. Rev. B* **86** 155307